A qualitative difference in decision-making of rats vs. humans explained by quantitative differences in behavioral variability

Quynh Nhu Nguyen and Pamela Reinagel*
Division of Biological Sciences, Section of Neurobiology, University of California San Diego, 9500 Gilman Drive, La Jolla CA 92093-0357.
*to whom correspondence should be addressed: preinagel@ucsd.edu

Abstract

When observers make rapid, difficult sensory decisions, their reaction time is highly variable from trial to trial. We previously compared humans and rats performing the same visual motion discrimination task. Their reaction time distributions were similar, but for humans accuracy was negatively correlated with reaction time, whereas for rats it was positively correlated. This is of interest because different mathematical theories of decision-making differ in their predictions regarding the correlation of accuracy with reaction time. On the premise that sensory decision-making mechanisms are likely to be conserved in mammals, our objective is to reconcile these results a common theoretical framework. A bounded drift diffusion model (DDM) with stochastic parameters is a strong candidate, because it is known to be able to produce either late errors like humans, or early errors like rats. We consider here such a model with seven free parameters: the evidence accumulator's starting point z, drift rate v, non-decision time t, threshold separation a, and three noise terms σz, σv, and σt. We fit these parameters to data from both rats and humans. Trial data simulated by the model recapitulate quantitative details of the relationship between accuracy and reaction time in both species. On this model, the species difference can be explained by greater variability in the starting point of the diffusion process (σz) in rats, and greater variability in the drift rate (σv) in humans.

Keywords: Drift Diffusion Model; random dot coherent motion; rodent vision; collapsing bound.
Running title: "Different variability in human and rat decision-making"
Number of pages: 16
Number of figures: 8
Words in abstract:229
Words in introduction: 682
Words in discussion:685
Conflict of Interest: The authors declare no competing financial interests
Acknowledgements: Support for this research was provided by a Kavli Institute for Brain and Mind Innovative Research Grant IRG2013-007 and the Regents of California Academic Senate Bridge Fund R0034B. Carly Shevinsky shared human subject data in advance of publication.

Introduction

One might expect decision making by humans to be quite different from that of rats. In decisions with wide-reaching long-term consequences, we expect (or at least wish) humans would avail themselves of abstract conceptual thought, logical reasoning, and culturally accumulated knowledge that would be unavailable to a rat. Yet all organisms face a continuous challenge of selecting among alternative available actions in order to pursue goals. In order to select an action, sensory information, internal knowledge, and goals are combined to assess and evaluate the likely outcomes of possible actions relative to survival needs. Often the information is incomplete, but time is limited, so an action must be selected despite unresolved or unresolvable uncertainty. When it comes to the continuous sensory guidance of moment-by-moment actions, even humans rely on a largely implicit, rapid, automated processing. Some mechanism is needed to ensure timely commitment and to optimize outcome on average, and this must adapt flexibly to prevailing sensory context, shifting goal priorities, the urgency of action, and the severity of consequences of errors. These mechanisms are likely to be conserved across mammals.

A now-classic series of studies in humans and non-human primates introduced the use of a stochastic visual motion task to study decision making (Britten et al., 1992; 1993; Britten et al., 1996; Shadlen et al., 1996; Shadlen and Newsome, 1996; Gold and Shadlen, 2001; Shadlen and Newsome, 2001; Mazurek et al., 2003; Huk and Shadlen, 2005; Palmer et al., 2005; Gold and Shadlen, 2007). In each trial a visual stimulus provides information regarding which of two available actions is associated with reward and which is associated with non-reward or penalty. As stimulus strength increases, accuracy increases and reaction time decreases for both monkeys (Roitman and Shadlen, 2002) and humans (Palmer et al., 2005). This is parsimoniously explained by drift diffusion models, which postulate that noisy sensory evidence is integrated over time until the accumulated evidence reaches a decision threshold (Stone, 1960; Ashby, 1983; Busemeyer and Townsend, 1993; Gold and Shadlen, 2001; Usher and McClelland, 2001; Palmer et al., 2005; Gold and Shadlen, 2007; Brown and Heathcote, 2008; Ratcliff and McKoon, 2008; Ratcliff et al., 2016).

Although this class of model is highly successful, more data are needed to test model predictions and differentiate among competing versions of the model or alternative model classes (Wang, 2002; Ratcliff and McKoon, 2008; Pleskac and Busemeyer, 2010; Purcell et al., 2010; Rao, 2010; Heathcote and Love, 2012; Huang et al., 2012; Tsetsos et al., 2012; Huang and Rao, 2013; Usher et al., 2013; Scott et al., 2015; Ratcliff et al., 2016; Sun and Landy, 2016; White et al., 2018).

When monkeys perform this task, among trials of the same stimulus strength the interleaved trials with longer reaction times are more likely to be errors. In its simplest form the drift diffusion model does not explain this result; therefore the observation has been an important constraint for recent theoretical efforts. The result can be explained if the decision bound is not constant but instead decays as a function of time (Bowman et al., 2012; Drugowitsch et al., 2012). A collapsing decision bound can be rationalized as an optimal strategy under some task constraints (Rao, 2010; Hanks et al., 2011; Huang and Rao, 2013; Tajima et al., 2016) though this argument has been challenged by others (Hawkins et al., 2015; Boehm et al., 2016). There are alternative ways to explain the data within the drift diffusion model framework without positing an urgency signal or decaying bound (Ditterich, 2006a; b; Ratcliff and McKoon, 2008; Ratcliff and Starns, 2013).

In the interest of developing a rodent model for perceptual decision-making, we trained rats to perform the random dot motion task (Reinagel, 2013). Rats differed from humans and other primates in one key respect: for rats, later decisions are more likely to be accurate (Reinagel, 2013; Shevinsky and Reinagel, 2019). This result is not readily explained by some models suggested to explain the late errors of primates. The purpose of this study is to test one variant of the drift-diffusion model for its ability to explain data from both species.

Results

1. Drift Diffusion Model with Static Parameters

In a basic drift diffusion model, the relative sensory evidence in favor of a decision (e.g. "motion is rightward" vs. "motion is leftward") is accumulated by an internal decision variable, resulting in a biased random walk, i.e., diffusion with drift (Fig. 1A). The strength of the drift is determined by the sensory signal to noise ratio (e.g. motion coherence). When the decision variable reaches either decision threshold, the agent commits to a choice. The time at which the decision variable crosses a threshold (reaction time), and the identity of the decision threshold that is crossed (correct vs. incorrect), vary from trial to trial; the distribution of reaction times and the probability of correct response depend on the drift rate and the starting point of the integrator. The asymmetric shape of the reaction time distribution (Fig. 1B) resembles that observed in experimental data.

In this simple form, the drift diffusion model depends on only four parameters: the threshold separation ***a***, non-decision time ***t***, accumulator starting point ***z***, and drift rate ***v*** (Fig. 1C). The experimental data that constrain these parameters are the accuracy (percent of decisions that are correct) and the shape of the distribution of reaction times, for each stimulus strength tested.

An interesting feature of this model is that for any given stimulus strength and decision threshold, errors and correct responses have the same reaction time distributions (Fig. 1B, red vs. green). Errors are on average the same speed as correct responses, even if the signal is so strong that errors are very rare. Therefore the accuracy of the decision is independent of RT.

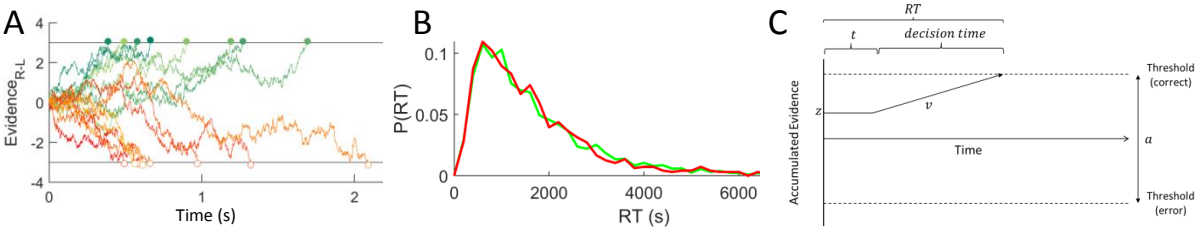

Figure 1. Properties of Basic Drift Diffusion Model. A. Noisy sensory evidence is integrated over time, resulting in a random walk in each trial; a decision occurs when the accumulated evidence reaches one of the decision thresholds. The traces show eight randomly chosen example trials that terminated in correct decisions (greens) and eight that terminated in error decisions (reds). Although an equal number are shown, the signal strength resulted in 97% correct decisions in the condition illustrated. **B.** Reaction time distributions for errors (red) vs. correct trials (green) of trials simulated as in A. Each distribution sums to 1. **C.** Definition of parameters for a formal drift diffusion model. The parameter a is the distance between the error and correct thresholds. The starting point, z, is expressed as a fraction of a, such that $z = 0.5$ is an unbiased or neutral starting point. The drift rate, v, depends on the sensory signal strength. These parameters are constant during a trial and across all trials of the same stimulus strength. The observable outcome is reaction time RT, and decision (correct or error). The non-decision time t reflects both sensory latency and motor latency, but is drawn at time $t = 0$ for graphical simplicity. Decision time is defined as $RT - t$. For the simulations illustrated in A, $t = 0$.

Both humans and rats deviate systematically from the prediction that correct and error trials have the same probability distribution, however. In the random dot motion coherence task, for example, correct trials of rat subjects are more likely to have longer reaction times compared to errors (Fig. 2A). If we compare the reaction time of each error trial to the temporally closest correct trial of the same coherence (Shevinsky and Reinagel, 2019), we see that on average, correct trials have longer reaction times than neighboring error trials of the same coherence (Fig. 2B). This trend is found in most individual experiments on rats (Fig. 2C). If one analyzes accuracy as a function of reaction time within a near-threshold coherence, the slope is positive (Fig. 2D), indicating that accuracy is increasing with RT.

Humans also violate the model prediction, but in the opposite way. For humans, errors are more likely to have long reaction times (Fig. 2E). On average correct trials have shorter reaction times than adjacent error trials of the same coherence (Fig. 2F). This effect is found in most individual experiments on humans (Fig. 2G). The slope of accuracy vs. reaction time is negative (Fig. 2H); in other words, accuracy declines with RT. This result been widely reproduced in studies of both humans and monkeys.

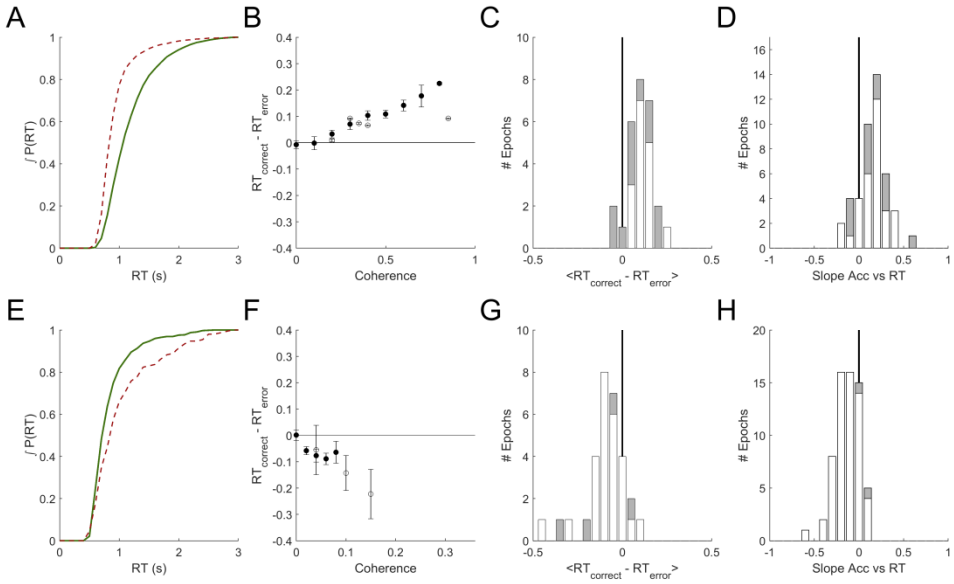

Figure 2. Summary of experimental data from rats (A-D) and humans (E-H). A. Cumulative probability function of reaction time for errors (maroon, dashed) and correct trials (olive, solid) for one example experiment in a rat, using a coherence for which the rat was ~85% correct. The maroon dashed curve is to the left, indicating that early responses are more likely to be errors. **B.** The average difference in reaction time between a correct trial and the temporally closest error trial of the same motion coherence; positive values indicate that correct trials had longer reaction times. This was computed within experimental epoch and then averaged over epochs. Coherences were randomly interleaved (closed symbols, N=31) or fixed within the epoch (open symbols, N=22). Error bars show SEM over epochs contributing data at that coherence. **C.** Distribution over epochs of the average difference between correct and error RT for coherences ≥0.4. Mixed coherence epochs (white, N=31) and fixed-coherence epochs (gray, N=11). **D.** Distribution over epochs of the slope of accuracy vs. RT for coherences with accuracy between 70-90%. Trials were divided into 6 quantiles of RT, and accuracy and mean RT computed within quantile. A line was fit to the resulting points for which mean RT was ≤1.5s and the slope of this line is reported. Mixed coherence epochs (white, N=31) and fixed-coherence epochs (gray, 13). **E.** Like A, for one example experiment in a human subject in which the subject was ~85% correct. **F.** Like B for human subjects (N=64 mixed coherence and N=4 fixed-coherence epochs). **G.** Like C, but for human subjects with coherences ≥0.04 (N=64 mixed coherence and N=4 fixed-coherence epochs). **H.** Like C, but for human subjects (N=64 mixed coherence and N=3 fixed-coherence epochs). Re-analysis of data from (Shevinsky and Reinagel, 2019).

We fit the basic drift diffusion model (Fig. 1C) to the behavioral data from both rats and humans. We used a hierarchical Bayesian estimation method (Wiecki et al., 2013), which yields species-level priors as well as individual-level values for each parameter: non-decision time ***t,*** drift rate parameters (***$v_1 \ldots v_n$***) for each coherence, and threshold separation ***a***. In the experiments, the correct response side was left or right with equal probability independently each trial, so it is impossible for the starting point of the diffusion process to be systematically biased towards the *correct* response threshold. Therefore we fixed the starting point bias ***z*** at 0.5 (no bias).

Threshold separations of humans and rats were similar (Fig. 3A; a_{human}= 1.62±0.35, a_{rat}= 1.62±0.22, mean±SD of population). Non-decision-time was longer for rats (Fig 3B; t_{human}=0.40±0.06 seconds, t_{rat}= 0.57±0.07 seconds). There is no reason to expect the non-decision times to be similar, as the motor response modality (key press vs. locomotion) are different. Humans and rats had similar drift rates (***v***) when the stimulus strength is expressed relative to the species threshold (Fig. 3C).

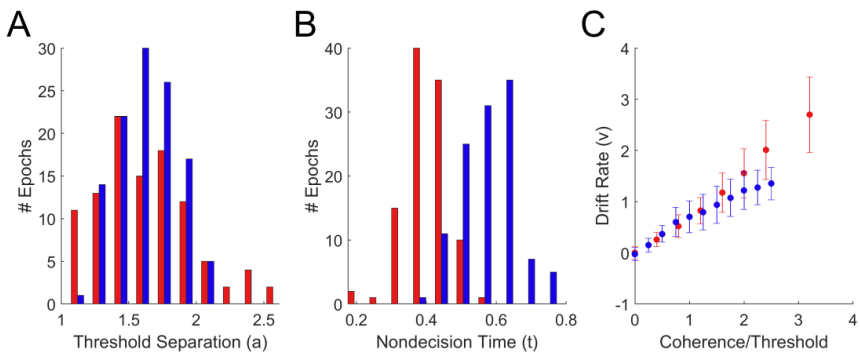

Figure 3. Recovered parameters of a basic Drift Diffusion Model fit to data from humans or rats. All trend-stationary epochs of all subjects were included (N=104 epochs from humans, red; N=115 epochs from rats, blue). **A.** Distribution of threshold separation a. **B.** Distribution of non-decision-time t. **C.** Drift rate parameter v (mean±SD over subjects) as a function of stimulus strength, expressed as motion coherence divided by the median coherence threshold of the species: 0.05 (humans) or 0.40 (rats). Threshold is defined as the coherence at which accuracy is 70%, derived from psychometric fit of the same experiments (Shevinsky and Reinagel, 2019). The starting point was constrained to be neutral with respect to the correct response ($z = 0.5$).

We used the parameters fit to each experimental epoch to simulate trials from the model, and subjected the simulated population data to the identical analysis as the real data. The model successfully fit the psychometric curves and the average reaction time distributions of individual subjects (not shown), but failed to replicate the difference between error and correct trials within condition for either humans or rats (Fig. 4). This result is expected, and serves as a baseline to which other models may be compared.

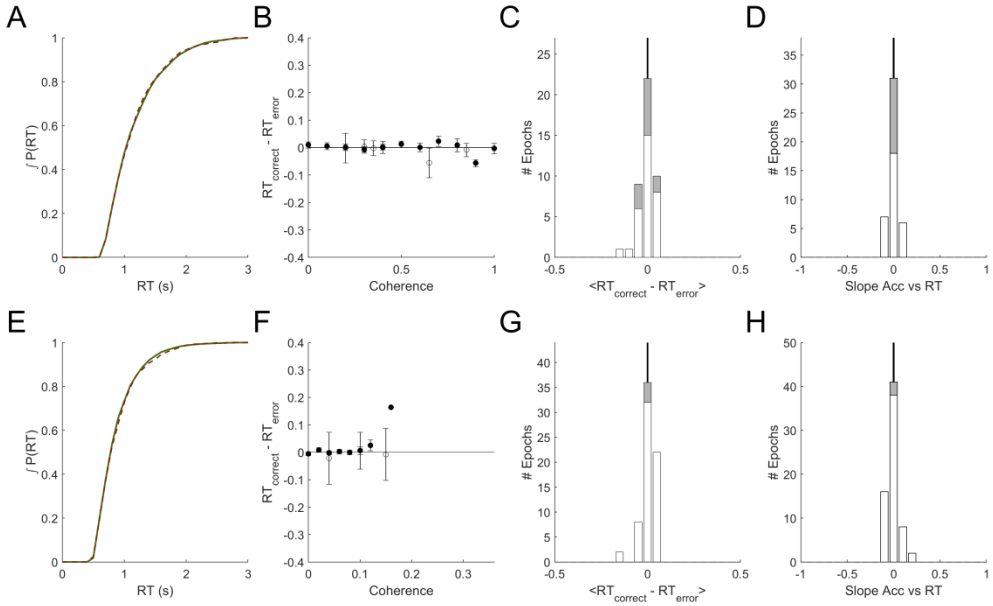

Figure 4. Basic DDM fails to replicate the interaction between elapsed time and accuracy in either species. A. Cumulative probability distributions of error vs. correct trials in simulated data for the same rat epoch analyzed in Fig. 2A. **B.** Difference in RT between correct and error trials as a function of coherence in simulated rat epochs, cf. Fig. 2B. **C.** Average RT difference in each simulated rat epoch, cf. Fig 2C. **D.** Slope of accuracy vs. RT, cf. Fig. 2E. **E-H.** Analysis of simulated human data, cf. Fig 2 E-H.

2. Drift Diffusion Model with Variable Parameters

It was previously shown that adding noise to the parameters of a bounded drift diffusion model can differentially affect the error and correct reaction time distributions (Ratcliff and McKoon, 2008). Depending on parameter values, this can produce either an increase or a decrease in accuracy as a function of reaction time. Therefore this model could account for both the human and rat results and provide a basis for understanding the difference between them. The stochastic parameter model we implemented has three additional parameters: variability in starting point σ_z, variability in non-decision time σ_t, and variability in drift rate σ_v (Fig. 5).]

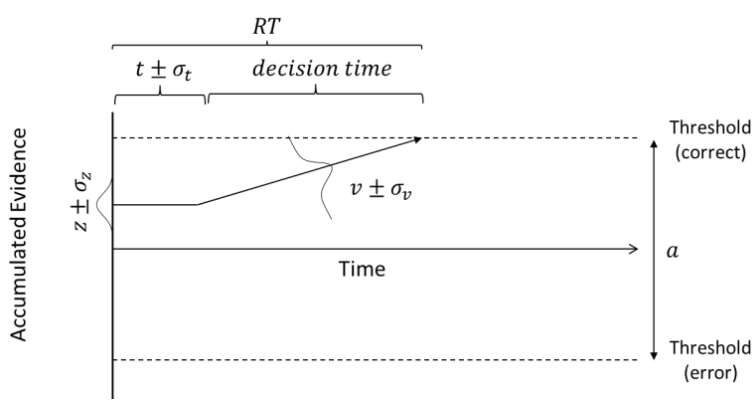

Figure 5. Addition of variability to the parameters of the drift diffusion model. Parameters t, z, and v in the drift diffusion model remain constant within a trial, but vary from trial to trial according to a normal distribution with standard deviations σ_t, σ_z and σ_v respectively. After (Ratcliff and McKoon, 2008).

In a preliminary analysis, a systematic sweep of the parameter space of this model revealed that whenever starting point variability σz was high relative to the threshold separation a, this model produced faster errors and slower correct responses, a trend that was enhanced when σv was low. Therefore we predicted that rats might have a high σz/a ratio with a low value of σv, which would explain our finding that rats' accuracy increases with reaction time, to an increasing degree as coherence increases. High drift rate variability σv produced late errors in the model, however, a tendency that was enhanced when threshold a was high and/or starting point variability σz was low. The strength of this effect increased with the drift rate v (simulations not shown, and (Ratcliff and McKoon, 2008)). Therefore we predicted that humans might have a high σv and low σz/a ratio, which could explain our finding that humans' accuracy decreases with reaction time, to an increasing degree as coherence increases. The parameter σt had no effect on whether accuracy increased or decreased with reaction time. Therefore we did not expect σt to affect the dependence of accuracy on elapsed time in either species, and had no basis for predicting it.

When we fit the model shown in Fig. 5 to the data set, we found that these added parameters improved the model fits of both species, even after accounting for the additional free parameters (DIC, not shown) and assessed by cross-validation using a 50/50 data split (shown below). The recovered parameter distributions over the populations are shown in Fig. 6.

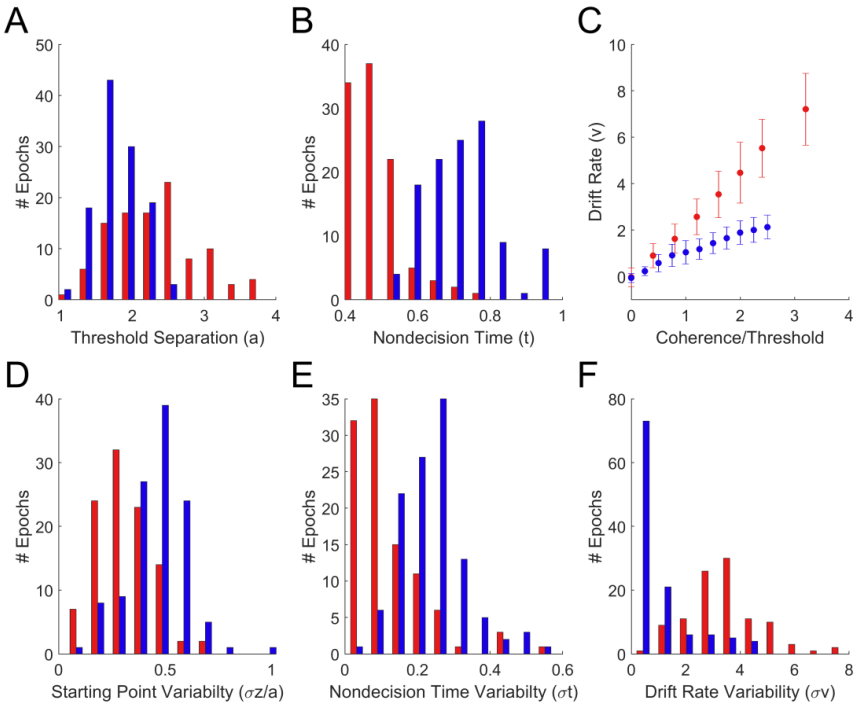

Figure 6. Recovered parameters of Drift Diffusion Model with noise terms fit to data from humans or rats. Data sets as in Fig. 3. Parameters fit to individual human (red) and rat (blue) experimental epochs. **A.** Distributions of threshold separation a: $a_{human} = 2.33 \pm 0.60$, $a_{rat} = 1.79 \pm 0.32$. **B.** Distributions of nondecision time t: $t_{human} = 0.48 \pm 0.07$ s, $t_{rat} = 0.72 \pm 0.10$ s. **C.** Drift rate v for each stimulus strength (mean±SD over subjects) where strength is given by coherence divided by species median coherence threshold, 0.05 (humans) or 0.40 (rats). **D.** Distributions of starting point variability parameter σz, expressed as a fraction of the threshold separation a: Human $\sigma z/a = 0.31 \pm 0.12$, rat $\sigma z/a = 0.46 \pm 0.14$. The raw parameter σz (not shown) was also higher for rats: $\sigma z_{human} = 0.68 \pm 0.18$, $\sigma z_{rat} = 0.81 \pm 0.22$. **E.** Distributions of nondecision time variability σt: Human $\sigma t_{human} = 0.12 \pm 0.10$, $\sigma t_{rat} = 0.24 \pm 0.09$. **F.** Distributions of drift rate variability parameter σv: $\sigma v_{human} = 3.42 \pm 1.37$, $\sigma v_{rat} = 0.93 \pm 1.13$.

According to this model, rats have a lower threshold separation ***a*** (Fig. 6A) as well as higher starting point variability σz (not shown) resulting in a higher $\sigma z/a$ ratio (Fig. 6D). This model also attributes a longer non-decision time ***t*** to rats than humans (Fig. 6B). Unlike the previous model, the drift rate was higher for humans than rats, even after normalizing the coherence to the species-average psychometric threshold (Fig. 6C). Rats had more variability in the non-decision time σt (Fig. 6E). Humans had greater drift rate variability σv than rats (Fig. 6F). These results qualitatively agreed with our predictions of a high $\sigma z/a$ ratio with low σv in rats, and a low $\sigma z/a$ ratio with high σv in humans.

The model was not explicitly optimized for its ability to account for rats' increase in accuracy with elapsed time or humans' decline in accuracy with elapsed time. To test whether it did so, we simulated trials for each subject based on their individual parameters in the variable parameter model (Fig. 6), and performed the identical analysis as for real data (Fig. 2) and the fixed-parameter model (Fig. 4). The model with noise parameters succeeded in capturing the interaction between elapsed time and accuracy in both species (Fig. 7).

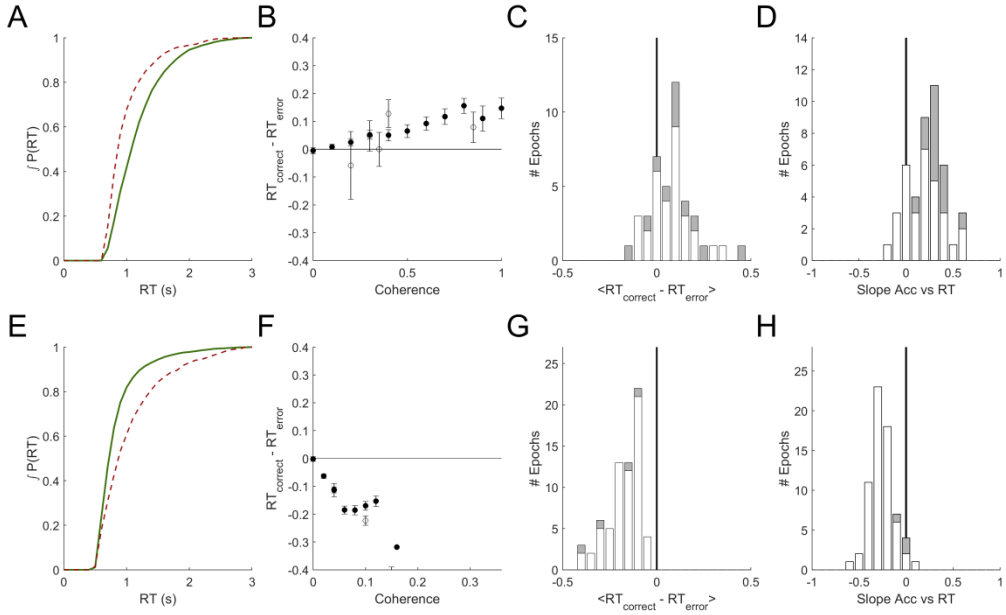

Figure 7. Simulated data from DDM with noise parameters. A-D simulations based on parameters fit to data from rats, **E-H** simulations based on parameters fit to data from humans. **A,E.** Cumulative reaction time distribution of simulated error trials (maroon, dashed) and correct trials (olive, solid) for the same example subject shown in Fig. 2A,E and 4A,E. **B,F.** Local reaction time difference between correct and error trials, computed on simulated trials within epoch, and averaged across epochs as described in Fig. 2B. **C,G.** Distribution across epochs of mean reaction time difference within epoch, as described in Fig. 2 C,G. **D,H**. Distribution over epochs of the slope of accuracy vs. reaction time, as described in Fig. 2 D,H.

3. Lesions of the model

To evaluate the contributions of the different noise parameters, we performed lesions within the model. The overall model fit was measured by the residual error between the real and predicted reaction time distributions using cross-validation data. This was computed separately for each coherence and summed over coherences. Here we can see that for individual subjects (Fig. 8 A,E) and over the population (Fig. 8 B,F) the model with all three noise parameters (+++, cf. Fig. 5) fit the data better than the model without any (---, cf. Fig. 1).

In single parameter "lesions" of the model, we re-simulated trials using the parameters fit to the full model (Fig. 6) after setting one of the noise parameters (σ_z, σ_t, or σ_v) to zero for all subjects. For rats, the average fit of the model was much worse if we ablated σ_z, compared to the ablation of either σ_t or σ_v (Fig. 8 A,B). For humans, the error was much worse if we ablated σ_v compared to either σ_z or σ_t (Fig. 8 E,F). Double lesion results were consistent with this: for rats the double-lesion model that retained only σ_z had the best fit; for humans the double-lesion keeping only σ_v had the best fit.

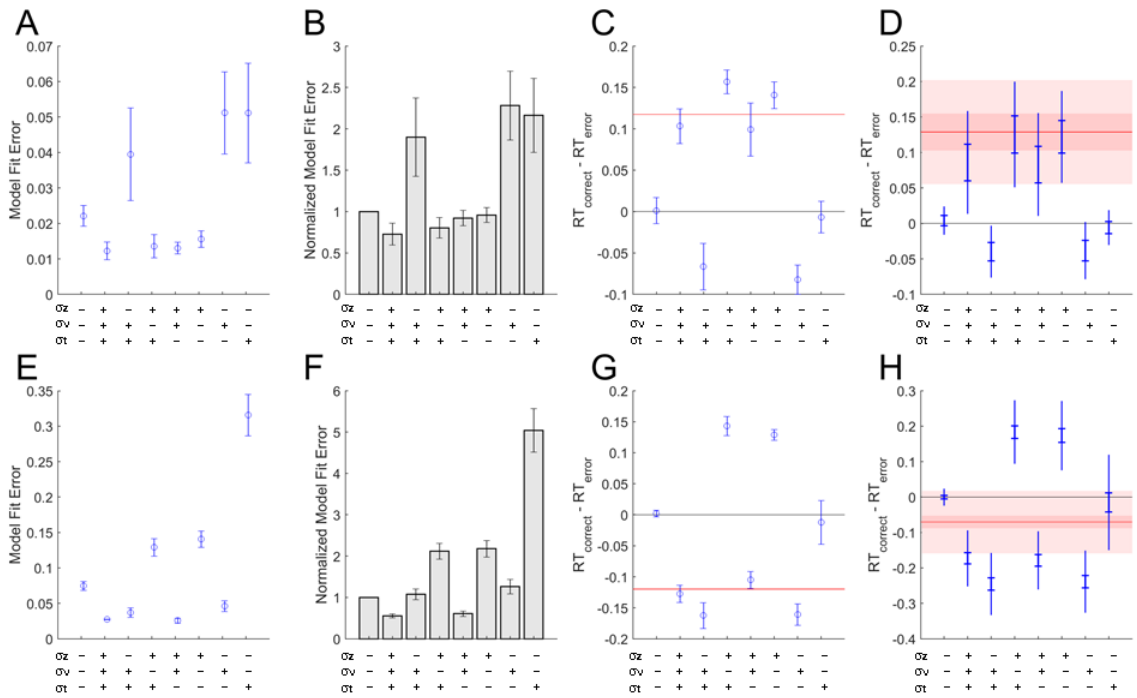

Figure 8. Effects of noise parameter ablations in the model. Results are shown for rats (top row) and humans (bottom row). Individual example subjects and population results for N=9 rats and N=31 humans. The leftmost column in each plot (---) shows results for the model that was fit without noise parameters (cf. Fig. 1,3,4). The second column (+++) represents the model that was fit with three noise parameters σz, σv and σt (Fig. 5-7). Remaining columns are results of simulations using parameters fit in the latter model, after selective ablation of noise parameters as indidcated below the panels. **A,E.** The cross-validation error of the model fit between simulated and real data for one example subject. Error bars indicate SEM over four independent model fitting runs. **B,F.** The cross-validation error normalized within subject to the error of the fit of the first model. Error bars represent MSE over population. **C,G.** The difference between the mean reaction time of correct trials and of errors, for same example subject shown in (A,E). Difference was calculated within coherence, for all coherences for which subject's accuracy was between 70-90% correct, then averaged over coherences. Error bars indicate SEM over four independent runs. Red line indicates the result from the data. **D,H.** Difference between correct and error reaction times computed as in (C,G) within subject, summarized over population. Red line, dark and light shading represent the mean, MSE and SD over the population for the original data. Thick blue bars and horizontal hatches show population mean±MSE; thin blue whiskers show population SD. This figure includes only one psychometric epoch from each subject. Similar results were found including all epochs from all subjects (not shown).

To assess the interaction between elapsed time and accuracy, we computed the difference between the mean reaction times of correct and error trials of the same coherence, $\langle RT_{correct} \rangle - \langle RT_{error} \rangle$. The model with all three noise parameters (+++) replicated the fact that for rats, errors had shorter reaction times (Fig. 8 c-d). Ablating σ_v from the model resulted in this effect being

overestimated; ablating σ_z abolished this property and uncovered a weak opposite effect; ablating σ_t was inconsequential. We infer that starting point variability is the model parameter that specifically accounts for rats' increasing accuracy with reaction time; but this coexists with a weaker effect in the opposite direction due to drift rate variability.

This model also replicated the trend that human errors have longer reaction times, but overshot the magnitude of the real effect (Fig. 8 g-h). Ablating σ_z caused the trend to be further overestimated; ablating σ_v caused the model to predict the opposite effect instead; ablating σ_t was inconsequential. We infer that drift rate variability is the model parameter responsible for reproducing humans' declining accuracy with reaction time; but this coexists with a weaker effect in the opposite direction due to starting point variability.

Note that the interaction between accuracy and reaction time is a small effect, compared to the very large effect of coherence on the percent correct (psychometric curve) and the average reaction time (chronometric curve), all of which the model is simultaneously fitting. The model parameters that provide the best fit to the data overall are not necessarily those that produce the best fit of the interaction between accuracy and elapsed time. This may explain why the magnitude of the effect is not exactly replicated.

Discussion

The drift diffusion model with noise parameters (Ratcliff and McKoon, 2008) can parsimoniously account for the interaction between accuracy and reaction time in both species, without explicitly positing an urgency signal or collapsing bound. This provides a unified way to understand the behavior in both species and a common framework to compare them.

Within the framework of this model, the species difference can be attributed to a combination of higher starting point variability in rats, and higher drift rate variability in humans. But both species have variability in both starting point and drift rate, contributing opposing effects that balance to produce the observed net effect in each species. The parameter distributions in rat and human populations overlapped considerably. Thus the qualitative difference in behavior (Fig. 2) could be explained by subtle quantitative differences in the same underlying decision-making algorithm.

A static response bias would manifest as starting point variability in this model. For example, a bias to respond "L" would result in a starting point z that is closer to the correct decision threshold in left-motion trials, but further from it in R-motion trials. We note that high σz was found in rats even when overtly biased subjects were excluded from the analysis, however. Starting point variability could also be caused by history-dependent biases. It is known that responses can be biased by the previous trial's stimulus, response, and outcome in mice (Busse et al., 2011), rats (Lavan et al., 2011), non-human primates (Sugrue et al., 2004), and humans (Goldfarb et al., 2012), see (Frund et al., 2014). These factors may partly explain the starting point variability in both species, and may be more pronounced in rats. One might search for neural correlates of such a bias in motor planning or salience map areas.

We speculate that variability from trial to trial in the drift rate could be caused by changes in general arousal or selective or non-selective visual attention. For example if arousal or attention increased baseline firing rates or evoked responses or reduced noise correlations among motion-selective neurons in extra-striate cortex, this would be expected to increase the rate of accumulation of

evidence in downstream parietal neurons. If attention has stronger effects or varies more from trial to trial in primates than rodents, this could lead to a species difference in σ_v.

Although non-decision-time variability was not crucial to explaining the species difference of interest here, the model indicates that rats have more non-decision-time variability. Confidence judgements may play a role in this (Kepecs et al., 2008; Ratcliff and Starns, 2013).

In summary, this model implicates an important role for behavioral variability in explaining the species difference we investigated. We do not find that one species' behavior is more variable than the other, but rather that different types of variability are found in different proportions. We do not mean to imply that such behavioral variability is either random or dysfunctional. It is possible that non-sensory influences shift the decision process from trial to trial in a systematic and reproducible fashion that could be functionally adaptive in the context of natural behavior. Locations and very recent experiences are likely to be informative about the expected rewards for behaviors in the wild, even though we have broken those spatial and temporal correlations in our laboratory task.

On the premise that basic mechanisms of perceptual decision-making are likely to be conserved, fitting a single model to data from multiple species – especially where they differ – may be a powerful way to develop and distinguish among alternative computational models. If the differences between species are merely quantitative differences in a conserved underlying algorithm, it may be advantageous to study a given aspect of the computation in a species that has particularly high or low variability in a certain parameter.

We have explored one model that can explain our data from both species, but other models may also be able to account for the same data in other ways, potentially making distinct testable predictions for future experiments. To enable such direct comparisons, the entire dataset analyzed in this paper will be made available in a data repository upon publication.

Methods

Experimental Data

All human and rat data modeled in this manuscript were previously described (Shevinsky and Reinagel, 2019). Briefly, the task was random dot coherent motion discrimination. The stimulus parameters other than coherence (e.g. dot size, dot density, motion speed, contrast) were adjusted for each species to ensure that accuracy ranged from chance (50%) to perfect (100%) and reaction times ranged from ~500-2500ms for typical subjects of the species. Human or rat subjects voluntarily initiated each trial by a central keypress or lick respectively. This immediately triggered a random dot motion display on a computer monitor, with coherent motion either to the left or right, persisting until the subject responded. Subjects could respond at any time by a left vs. right keypress or lick. Responses on the side toward which the coherent dots were moving were rewarded with money or water. Responses on the opposite side were penalized by a brief time-out. Learning trials were exluded from analysis. Remaining trial data from each subject were broken into "epochs" during which the task was not changed and the subject's behavior (accuracy, reaction time) was not trending. For additional details see (Shevinsky and Reinagel, 2019).

The data set included 115 epochs from 18 individual rats, for 274,170 total rat trials, and 104 epochs from 64 individual human subjects, for 151,828 total human trials. Experimental data with

and/or bias were included. The data were organized into three training data sets for each species: all epochs, all fixed coherence epochs, and the single best unbiased psychometric epoch of each subject. The "fixed coherence" epochs are those in which coherence was not varied during the experiment; this condition was tested frequently in rats, but rarely in humans. Selection criteria for "best unbiased psychometric epoch" of a subject were: ≥500 trials, ≥4 coherence values, <10% difference in either accuracy or probability of L vs R responses at highest coherence; minimal temporal fluctuation in accuracy or reaction time; and if multiple epochs passed all these criteria, the one with the most trials. Note that absence of lapse or the relationship between reaction time and accuracy were not criteria.

Computational methods

Model fitting

General overview

Models were fit with the HDDM package in Python (Wiecki et al., 2013). The objective function for fitting is to maximize the likelihood of the observed reaction time distributions, evaluated separately at each coherence and distinguishing error trials from correct trials. Different model parameters were fit for each epoch because distinct epochs from the same subject differed in task parameters and/or average performance metrics. The models were trained for 100,000 iterations or upon evident convergence if sooner. Convergence was assessed by examining the asymptotic behavior over training iterations of each parameter value and of the deviance information criterion (DIC), as described in (Wiecki et al., 2013). A model was fit to a given data set at least twice and typically 5 times. These models converged to highly consistent DIC and parameter values on repeat runs.

The total number of model parameters was at most 1485 (human) or 1217 (rats), including the species-level priors, epoch-specific values for each parameter, independently fitting a drift rate ***v*** for every coherence, and including the three noise parameters (Figs 5-7). Note that the model is hierarchical: the species-level priors are constrained by and constrain the individual-level parameters of that species. Therefore there are fewer true degrees of freedom than the number of parameters. The number of data points greatly exceeded the number of parameters in both species: 102 trials/parameter (humans) or 225 trials/parameter (rats). The rat data and human data were fit separately in parallel for speed. This also allowed the species priors to have different standard deviations; otherwise in the HDDM software the widths of group priors are constrained to be the same across groups.

Anectdotally we found that after fitting, smoothing the curve relating coherence to drift rate v could improve model simulations. We conclude that imposing a smoothness constraint or a parametric form for this relationship within the model fit would be a helpful future improvement, but we did not implement this. All simulations presented in the paper were performed without such smoothing.

Models were also trained on only the even- or odd- numbered rows of a data set, using the other half of the data for cross-validation comparison to the simulated data. Parameters for odd vs. even data splits were often reproducibly slightly different, compared to the run-to-run variability of the parameters for the same data half. Nevertheless, the residual error of model fits to training vs. testing data sets were similar, suggesting that overfitting was not an issue for these models. Therefore, for Fig 2, 3-4 and 6-7, the properties shown were computed from the entire data set, or from a very large

number of simulated trials from a model fit to the entire data set. In Fig. 8 cross-validation errors are presented.

Modeling details

The drift diffusion process was simulated according to the equation $X(t) = X(t-1) \pm \delta$ with probability p of increasing and $(1-p)$ of decreasing (Milosavljevic et al., 2010). Here t is the time point of the process, with time step τ in seconds; $\delta = \sigma \cdot \sqrt{\tau}$ denotes the step size, where σ is the standard deviation of the Gaussian white noise of the diffusion; $p = 0.5 \cdot \left(1 + v \cdot \frac{\sqrt{\tau}}{\sigma}\right)$, where v is the drift rate. To be consistent with the simulation done by the HDDM package (Wiecki et al., 2013), the values for τ and σ were set at 0.1 msec and 1, respectively.

For any trial, the process starts at a starting position z, sampled from a uniform distribution of range σz, assumes a constant drift rate v, sampled from a normal distribution of standard deviation σv, and continues until $X(t)$ exceeds either threshold boundary. The non-decision-time t, sampled from a uniform distribution of range σt, is added to the elapsed time to obtain the final RT associated with that trial.

To retrieve the model parameters from experimental data, i.e. reaction time and accuracy, the HDDM package was used. The input data was first formatted as comma-separated files with the following mandatory columns: 'subj_idx', 'rt', and 'response', which correspond to the epoch number, reaction time, and accuracy, respectively. The main command was either 'HDDM', if no variability parameters were included, or 'HDDMTruncated', which allows for subject-level estimates of the variability parameters σz, σv, and σt.

Aside from the default parameters a, v, and t, additional parameters can be fitted with the 'include' keyword argument to the fit command. Otherwise, z is defaulted to be 0.5, and the variability parameters are defaulted to zero. Additionally, any parameter can be fitted according to some specific condition(s) using the 'depends_on' keyword argument, as long as the input data file contains information about those conditions. For example, we always let the drift rate v depend on 'coherence' so that the model fit will return a separate drift rate estimate for each coherence value.

Cross-validation Error Estimation

To determine the model fit error on cross-validation, models were fit separately to either the even rows or odd rows of the data file. The model parameters were used to simulate 1,000 trials per coherence. Any trials with simulated $RT > 3\ s$ were excluded from analysis. To distinguish error from correct trials, the reaction times of error trials were coded as negative values. Reaction times were then discretized into 0.25s bins. For each coherence separately, the reaction time distribution was computed. Thus a single probability distribution for each coherence summarized both the proportion of trials that were errors, and the shape of the RT distributions of errors and correct trials considered separately. The data from either the odd or even rows of the data set were used to generate reaction time distributions of training and cross-validation data in the same manner. Only coherences with at least 80 trials both the training and cross-validation data sets were included in the error estimate. The error was defined as the squared difference between the data and the model reaction time distributions, summed over reaction time bins and over qualifying coherences. The absolute value of the error is sensitive to the number of trials and the binning of reaction times (some of the mismatch between model and data is sampling noise). But those factors are constant for all the models, so comparisons are valid. Two separate training runs on each half of the data set were evaluated; the average over the four cross-validation error estimates is reported.

Local reaction time difference analysis

In Figs 2, 4 and 7, panels B,C,F, and G we measure the interaction between accuracy and reaction time using the temporally local measure $\langle RT_{correct} - RT_{error} \rangle$ introduced in (Shevinsky and Reinagel, 2019). Instead of comparing the reaction time distributions of errors and correct trials of the same coherence estimated from the entire epoch, we compare the reaction time of each error trial to a temporally adjacent correct trial of the same coherence (requiring a minimum distance of 3 trials to avoid sequential effects). This method is preferred because it is robust to non-trending non-stationarities that are commonly present in both human and rat data, not detected by traditional stationarity tests, and that could confound estimation of the effect of interest. In the case of model simulations, however, the time series are stationary by construction, so we used the difference between averages $\langle RT_{correct} \rangle - \langle RT_{error} \rangle$.

References

Ashby, G. (1983). A biased random walk model for two choice reaction times. *Journal of Mathematical Psychology* 27**,** 277-297.

Boehm, U., Hawkins, G.E., Brown, S., van Rijn, H., and Wagenmakers, E.J. (2016). Of monkeys and men: Impatience in perceptual decision-making. *Psychon Bull Rev* 23(3)**,** 738-749. doi: 10.3758/s13423-015-0958-5.

Bowman, N.E., Kording, K.P., and Gottfried, J.A. (2012). Temporal integration of olfactory perceptual evidence in human orbitofrontal cortex. *Neuron* 75(5)**,** 916-927. doi: 10.1016/j.neuron.2012.06.035.

Britten, K.H., Newsome, W.T., Shadlen, M.N., Celebrini, S., and Movshon, J.A. (1996). A relationship between behavioral choice and the visual responses of neurons in macaque MT. *Vis Neurosci* 13(1)**,** 87-100.

Britten, K.H., Shadlen, M.N., Newsome, W.T., and Movshon, J.A. (1992). The analysis of visual motion: a comparison of neuronal and psychophysical performance. *J Neurosci* 12(12)**,** 4745-4765.

Britten, K.H., Shadlen, M.N., Newsome, W.T., and Movshon, J.A. (1993). Responses of neurons in macaque MT to stochastic motion signals. *Vis Neurosci* 10(6)**,** 1157-1169.

Brown, S.D., and Heathcote, A. (2008). The simplest complete model of choice response time: linear ballistic accumulation. *Cogn Psychol* 57(3)**,** 153-178. doi: 10.1016/j.cogpsych.2007.12.002.

Busemeyer, J.R., and Townsend, J.T. (1993). Decision field theory: a dynamic-cognitive approach to decision making in an uncertain environment. *Psychol Rev* 100(3)**,** 432-459.

Busse, L., Ayaz, A., Dhruv, N.T., Katzner, S., Saleem, A.B., Scholvinck, M.L., et al. (2011). The detection of visual contrast in the behaving mouse. *J Neurosci* 31(31)**,** 11351-11361. doi: 10.1523/JNEUROSCI.6689-10.2011.

Ditterich, J. (2006a). Evidence for time-variant decision making. *Eur J Neurosci* 24(12)**,** 3628-3641. doi: 10.1111/j.1460-9568.2006.05221.x.

Ditterich, J. (2006b). Stochastic models of decisions about motion direction: behavior and physiology. *Neural Netw* 19(8)**,** 981-1012. doi: 10.1016/j.neunet.2006.05.042.

Drugowitsch, J., Moreno-Bote, R., Churchland, A.K., Shadlen, M.N., and Pouget, A. (2012). The cost of accumulating evidence in perceptual decision making. *J Neurosci* 32(11)**,** 3612-3628. doi: 10.1523/JNEUROSCI.4010-11.2012.

Frund, I., Wichmann, F.A., and Macke, J.H. (2014). Quantifying the effect of intertrial dependence on perceptual decisions. *J Vis* 14(7). doi: 10.1167/14.7.9.

Gold, J.I., and Shadlen, M.N. (2001). Neural computations that underlie decisions about sensory stimuli. *Trends Cogn Sci* 5(1)**,** 10-16. doi: S1364-6613(00)01567-9 [pii].

Gold, J.I., and Shadlen, M.N. (2007). The neural basis of decision making. *Annu Rev Neurosci* 30**,** 535-574. doi: 10.1146/annurev.neuro.29.051605.113038.

Goldfarb, S., Wong-Lin, K., Schwemmer, M., Leonard, N.E., and Holmes, P. (2012). Can post-error dynamics explain sequential reaction time patterns? *Front Psychol* 3**,** 213. doi: 10.3389/fpsyg.2012.00213.

Hanks, T.D., Mazurek, M.E., Kiani, R., Hopp, E., and Shadlen, M.N. (2011). Elapsed decision time affects the weighting of prior probability in a perceptual decision task. *J Neurosci* 31(17)**,** 6339-6352. doi: 10.1523/JNEUROSCI.5613-10.2011.

Hawkins, G.E., Forstmann, B.U., Wagenmakers, E.J., Ratcliff, R., and Brown, S.D. (2015). Revisiting the evidence for collapsing boundaries and urgency signals in perceptual decision-making. *J Neurosci* 35(6)**,** 2476-2484. doi: 10.1523/JNEUROSCI.2410-14.2015.

Heathcote, A., and Love, J. (2012). Linear deterministic accumulator models of simple choice. *Front Psychol* 3**,** 292. doi: 10.3389/fpsyg.2012.00292.

Huang, Y., Friesen, A.L., Hanks, T.D., Shadlen, M.N., and Rao, R.P.N. (2012). "How Prior Probability Influences Decision Making: A Unifying Probabilistic Model," in *Advances in Neural Information Processing Systems 25,* eds. P. Bartlett, F.C.N. Pereira, C.J.C.a.L. Burges, L. Bottou & K.Q. Weinberger. (Lake Tahoe, NV), 1277-1285.

Huang, Y., and Rao, R.P. (2013). Reward optimization in the primate brain: a probabilistic model of decision making under uncertainty. *PLoS One* 8(1)**,** e53344. doi: 10.1371/journal.pone.0053344.

Huk, A.C., and Shadlen, M.N. (2005). Neural activity in macaque parietal cortex reflects temporal integration of visual motion signals during perceptual decision making. *J Neurosci* 25(45)**,** 10420-10436. doi: 10.1523/JNEUROSCI.4684-04.2005.

Kepecs, A., Uchida, N., Zariwala, H.A., and Mainen, Z.F. (2008). Neural correlates, computation and behavioural impact of decision confidence. *Nature* 455(7210)**,** 227-231. doi: 10.1038/nature07200.

Lavan, D., McDonald, J.S., Westbrook, R.F., and Arabzadeh, E. (2011). Behavioural correlate of choice confidence in a discrete trial paradigm. *PLoS One* 6(10)**,** e26863. doi: 10.1371/journal.pone.0026863.

Mazurek, M.E., Roitman, J.D., Ditterich, J., and Shadlen, M.N. (2003). A role for neural integrators in perceptual decision making. *Cereb Cortex* 13(11)**,** 1257-1269.

Milosavljevic, M., Malmaud, J., Huth, A., Koch, C., and Rangel, A. (2010). The Drift Diffusion Model can account for the accuracy and reaction time of value-based choices under high and low time pressure. *Judgment and Decision Making* 5(6)**,** 437-449.

Palmer, J., Huk, A.C., and Shadlen, M.N. (2005). The effect of stimulus strength on the speed and accuracy of a perceptual decision. *J Vis* 5(5)**,** 376-404. doi: 10:1167/5.5.1.

Pleskac, T.J., and Busemeyer, J.R. (2010). Two-stage dynamic signal detection: a theory of choice, decision time, and confidence. *Psychol Rev* 117(3)**,** 864-901. doi: 10.1037/a0019737.

Purcell, B.A., Heitz, R.P., Cohen, J.Y., Schall, J.D., Logan, G.D., and Palmeri, T.J. (2010). Neurally constrained modeling of perceptual decision making. *Psychol Rev* 117(4)**,** 1113-1143. doi: 10.1037/a0020311.

Rao, R.P. (2010). Decision making under uncertainty: a neural model based on partially observable markov decision processes. *Front Comput Neurosci* 4**,** 146. doi: 10.3389/fncom.2010.00146.

Ratcliff, R., and McKoon, G. (2008). The diffusion decision model: theory and data for two-choice decision tasks. *Neural Comput* 20(4)**,** 873-922. doi: 10.1162/neco.2008.12-06-420.

Ratcliff, R., Smith, P.L., Brown, S.D., and McKoon, G. (2016). Diffusion Decision Model: Current Issues and History. *Trends Cogn Sci* 20(4)**,** 260-281. doi: 10.1016/j.tics.2016.01.007.

Ratcliff, R., and Starns, J.J. (2013). Modeling confidence judgments, response times, and multiple choices in decision making: recognition memory and motion discrimination. *Psychol Rev* 120(3)**,** 697-719. doi: 10.1037/a0033152.

Reinagel, P. (2013). Speed and accuracy of visual motion discrimination by rats. *PLoS One* 8(6)**,** e68505. doi: 10.1371/journal.pone.0068505.

Roitman, J.D., and Shadlen, M.N. (2002). Response of neurons in the lateral intraparietal area during a combined visual discrimination reaction time task. *J Neurosci* 22(21)**,** 9475-9489. doi: 22/21/9475 [pii].

Scott, B.B., Constantinople, C.M., Erlich, J.C., Tank, D.W., and Brody, C.D. (2015). Sources of noise during accumulation of evidence in unrestrained and voluntarily head-restrained rats. *Elife* 4**,** e11308. doi: 10.7554/eLife.11308.

Shadlen, M.N., Britten, K.H., Newsome, W.T., and Movshon, J.A. (1996). A computational analysis of the relationship between neuronal and behavioral responses to visual motion. *J Neurosci* 16(4)**,** 1486-1510.

Shadlen, M.N., and Newsome, W.T. (1996). Motion perception: seeing and deciding. *Proc Natl Acad Sci U S A* 93(2)**,** 628-633.

Shadlen, M.N., and Newsome, W.T. (2001). Neural basis of a perceptual decision in the parietal cortex (area LIP) of the rhesus monkey. *J Neurophysiol* 86(4)**,** 1916-1936.

Shevinsky, C.A., and Reinagel, P. (2019). The Interaction Between Elapsed Time and Decision Accuracy Differs Between Humans and Rats. *Front Neurosci* 13**,** 1211. doi: 10.3389/fnins.2019.01211.

Stone, M. (1960). Models for choice-reaction time. . *Psychometrika* 25 0**,** 251–226.

Sugrue, L.P., Corrado, G.S., and Newsome, W.T. (2004). Matching behavior and the representation of value in the parietal cortex. *Science* 304(5678)**,** 1782-1787. doi: 10.1126/science.1094765.

Sun, P., and Landy, M.S. (2016). A Two-Stage Process Model of Sensory Discrimination: An Alternative to Drift-Diffusion. *J Neurosci* 36(44)**,** 11259-11274. doi: 10.1523/JNEUROSCI.1367-16.2016.

Tajima, S., Drugowitsch, J., and Pouget, A. (2016). Optimal policy for value-based decision-making. *Nat Commun* 7**,** 12400. doi: 10.1038/ncomms12400.

Tsetsos, K., Gao, J., McClelland, J.L., and Usher, M. (2012). Using Time-Varying Evidence to Test Models of Decision Dynamics: Bounded Diffusion vs. the Leaky Competing Accumulator Model. *Front Neurosci* 6**,** 79. doi: 10.3389/fnins.2012.00079.

Usher, M., and McClelland, J.L. (2001). The time course of perceptual choice: the leaky, competing accumulator model. *Psychol Rev* 108(3)**,** 550-592.

Usher, M., Tsetsos, K., Yu, E.C., and Lagnado, D.A. (2013). Dynamics of decision-making: from evidence accumulation to preference and belief. *Front Psychol* 4**,** 758. doi: 10.3389/fpsyg.2013.00758.

Wang, X.J. (2002). Probabilistic decision making by slow reverberation in cortical circuits. *Neuron* 36(5)**,** 955-968.

White, C.N., Servant, M., and Logan, G.D. (2018). Testing the validity of conflict drift-diffusion models for use in estimating cognitive processes: A parameter-recovery study. *Psychon Bull Rev* 25(1)**,** 286-301. doi: 10.3758/s13423-017-1271-2.

Wiecki, T.V., Sofer, I., and Frank, M.J. (2013). HDDM: Hierarchical Bayesian estimation of the Drift-Diffusion Model in Python. *Front Neuroinform* 7**,** 14. doi: 10.3389/fninf.2013.00014.